Supplement of Atmos. Chem. Phys., 20, 6305–6321, 2020
https://doi.org/10.5194/acp-20-6305-2020-supplement

Atmospheric Chemistry and Physics
Open Access
EGU

Supplement of

Worsening urban ozone pollution in China from 2013 to 2017 – Part 1: The complex and varying roles of meteorology

Yiming Liu and Tao Wang

Correspondence to: Tao Wang (cetwang@polyu.edu.hk)

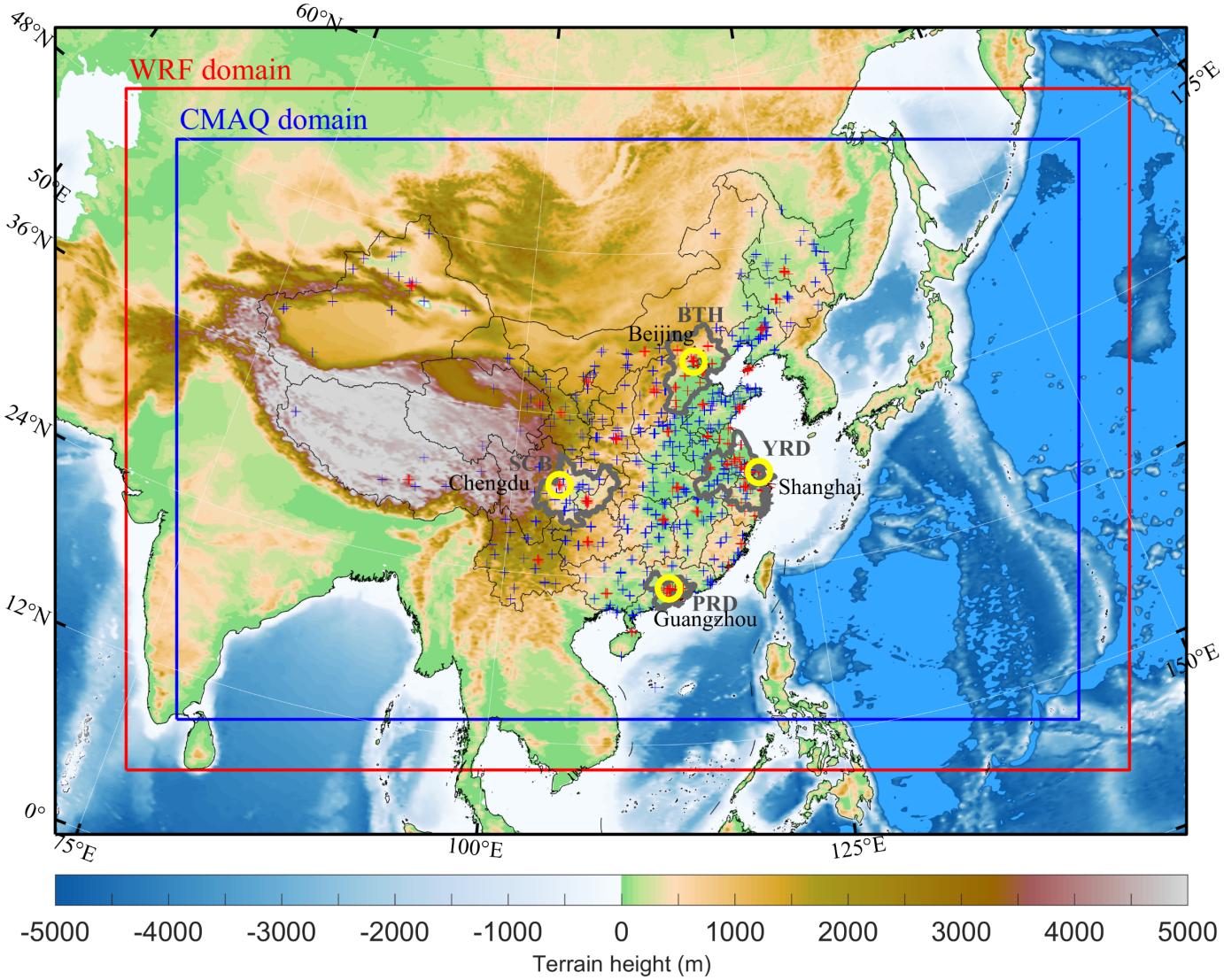

Figure S1 Model domains for the WRF (Red box) and CMAQ (Blue box) model. The red cross "+" represents the locations of 493 environmental monitoring stations in 74 cities which have been operational since 2013. The blue cross "+" represents the locations of new stations which were added in phases after 2014. The yellow circle denotes the locations of four major cities, Beijing, Shanghai, Guangzhou and Chengdu. The regions with bold gray boundary are the Beijing-Tianjin-Hebei (BTH), Yangtze River Delta (YRD), Pearl River Delta (PRD), and Sichuan Basin (SCB) regions.

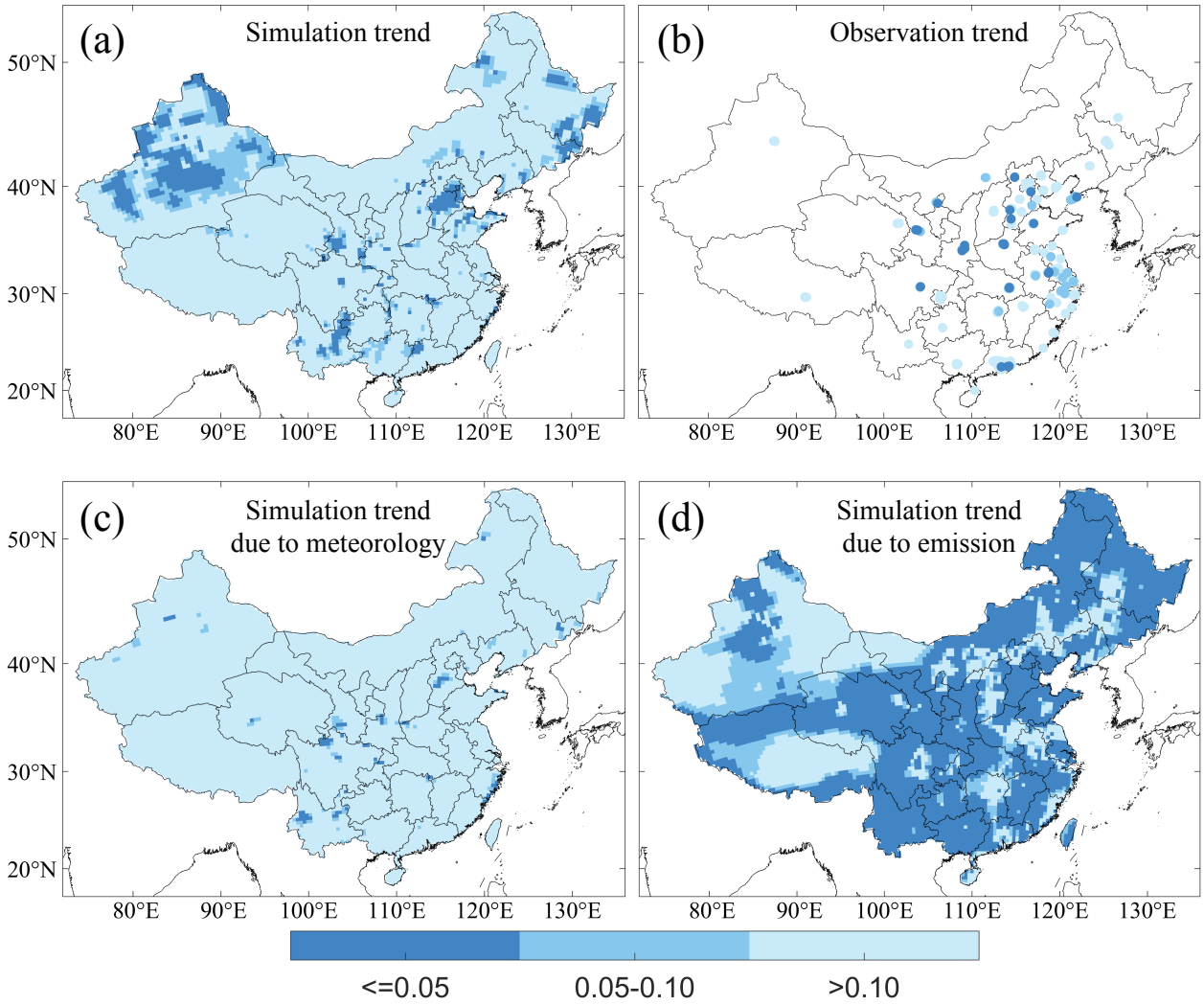

Figure S2 p values of regression for the rates of changes in the simulated (a) and observed (b) summer surface MDA8 O_3 mixing ratios, and those in the simulated values due to variations in meteorological conditions (c) and anthropogenic emissions (d) across land areas of China from 2013 to 2017.

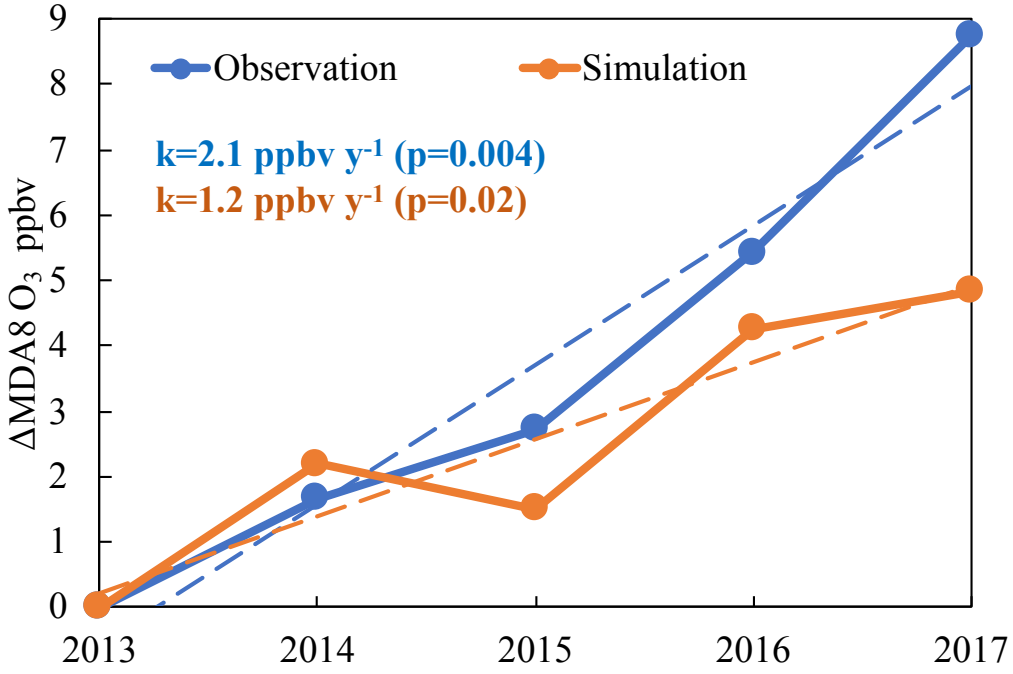

Figure S3 Changes in observed and simulated summer surface MDA8 O_3 mixing ratios averaged in 493 sites of 74 cities during 2013-2017 relative to those of 2013.

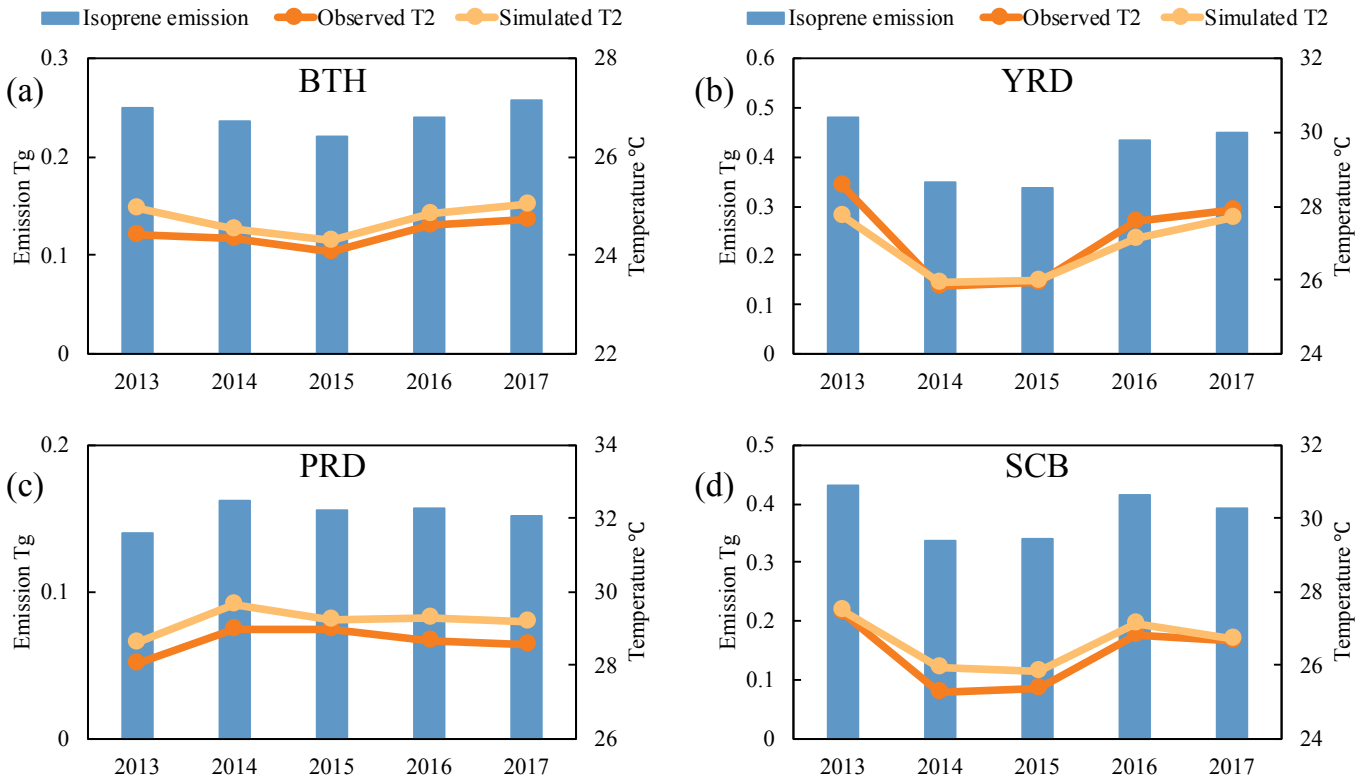

Figure S4 Variations in summer biogenic isoprene emissions, and observed and simulated temperature at a height of 2 m in the (a) Beijing-Tianjin-Hebei (BTH), (b) Yangtze River Delta (YRD), (c) Pearl River Delta (PRD), and (d) Sichuan Basin (SCB) regions from 2013 to 2017. The temperatures are averaged for the weather stations of the corresponding regions.

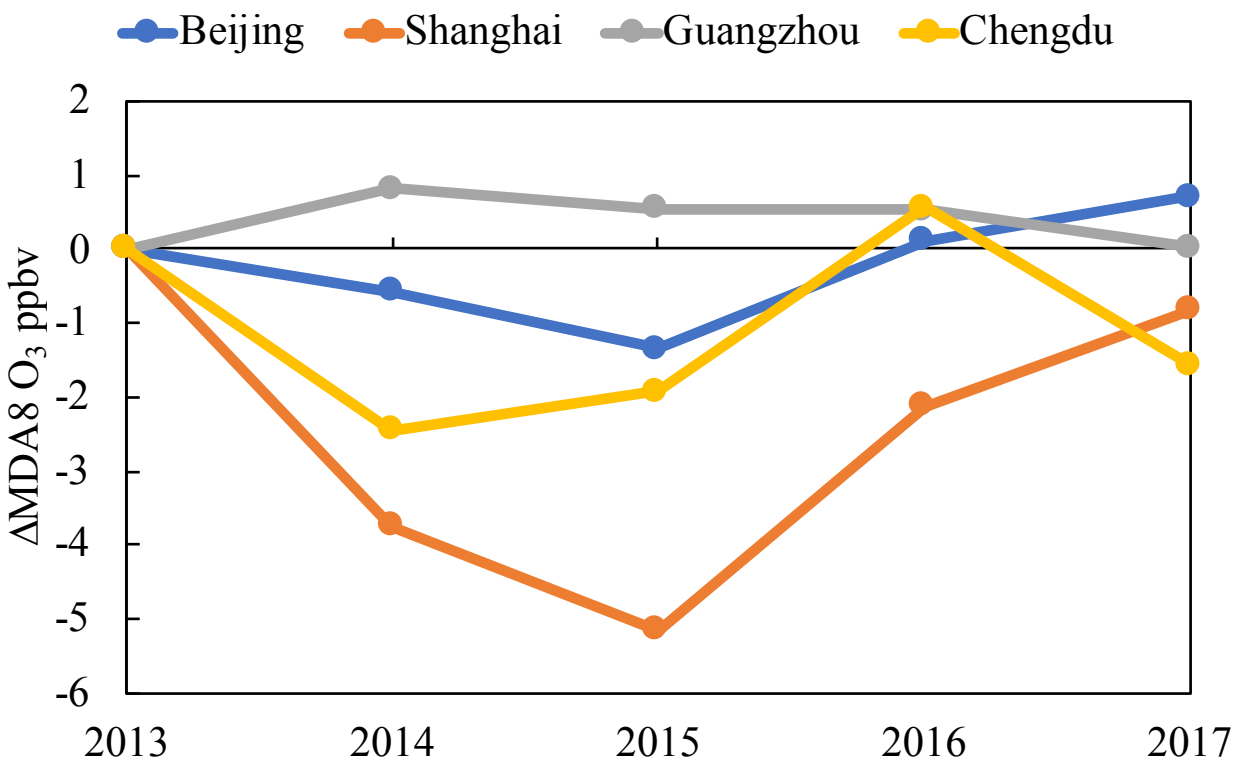

Figure S5 Changes in the simulated summer surface MDA8 O_3 due to variations in biogenic emissions in Beijing, Shanghai, Guangzhou, and Chengdu from 2013 to 2017 relative to 2013.

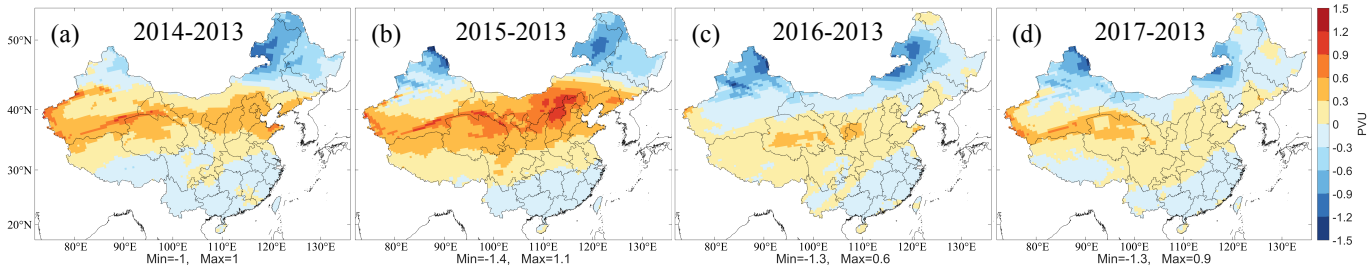

Figure S6 Changes in daytime averaged potential vorticity at a height of ~300 hPa (PVU: potential vorticity unit; 1 PVU=10^{-6} km^2 kg^{-1} s^{-1}) in summer from 2014 to 2017 relative to 2013.

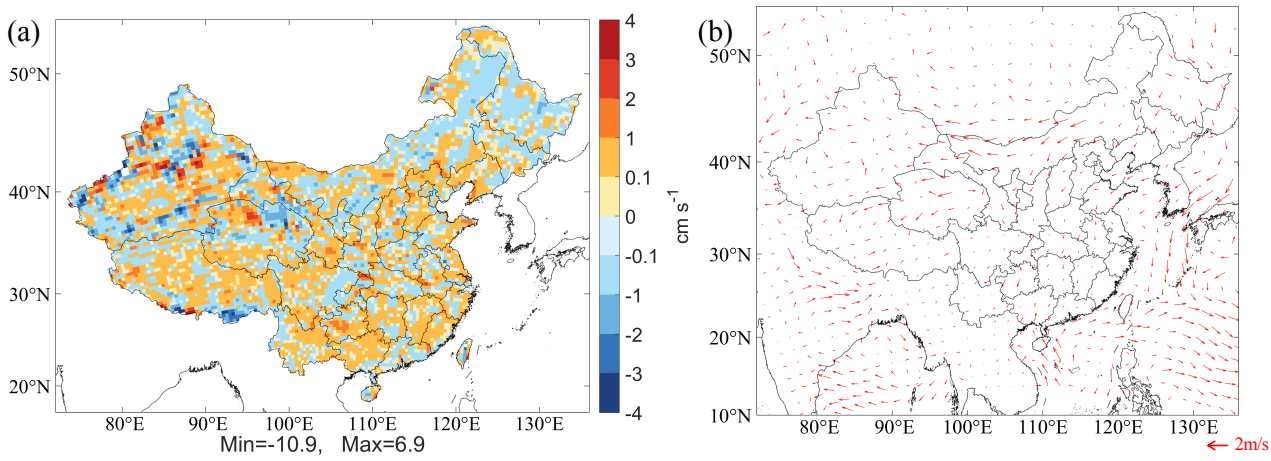

Figure S7 (a) Changes of daytime averaged vertical velocity at a height of ~850 hPa in summer of 2017 relative to that of 2013. (b) Changes of daytime averaged wind vector at the surface in summer of 2017 relative to that of 2013.

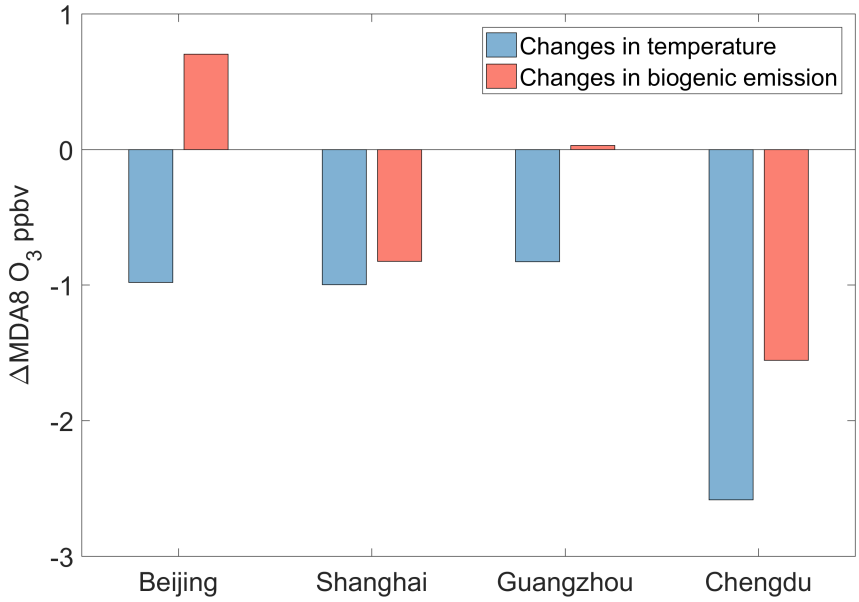

Figure S8 Changes in the simulated summer surface MDA8 O_3 mixing ratios due to the changes in temperature and biogenic emissions in 2017 relative to 2013 in Beijing, Shanghai, Guangzhou, and Chengdu.

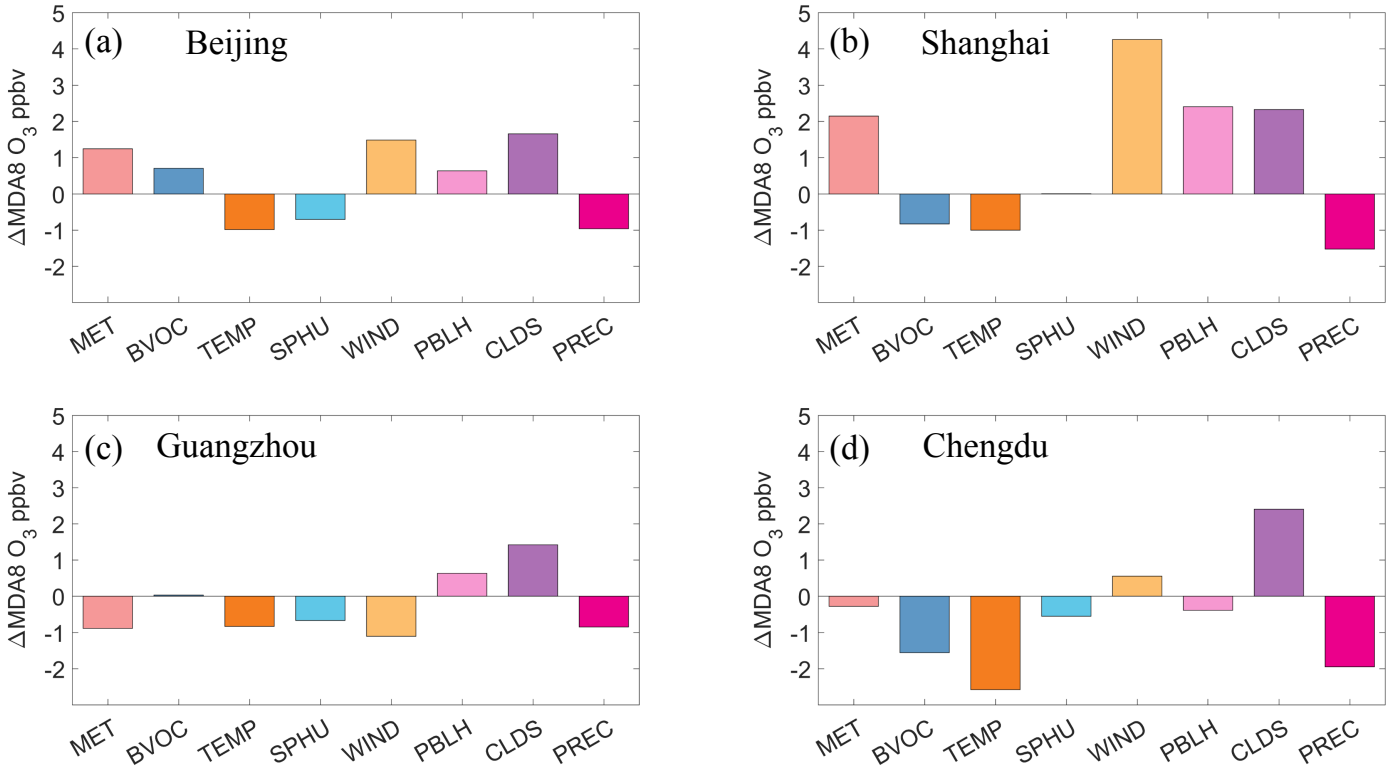

Figure S9 Changes in the simulated summer surface MDA8 O_3 mixing ratios in (a) Beijing, (b) Shanghai, (c) Guangzhou, and (d) Chengdu due to variations in various meteorological factors in 2017 relative to 2013, including meteorology (MET), temperature-dependent biogenic emissions (BVOC), temperature via changes in reaction rates (TEMP), specific humidity (SPHU), wind fields (WIND), planetary boundary layer height (PBLH), clouds (CLDS), and precipitation (PREC).

Table S1. Set-up of physical parameterization schemes for the WRF model

Item	Option
Microphysics scheme	Lin et al. scheme
Longwave radiation scheme	rrtm scheme
Shortwave radiation scheme	Goddard short wave
Surface-layer scheme	Revised MM5 Monin-Obukhov scheme
Land-surface scheme	Unified Noah land-surface model
Boundary-layer scheme	YSU scheme
Cumulus scheme	Kain-Fritsch (new Eta) scheme
Nudging options	Grid four-dimensional data analysis (FDDA)

Table S2. Heterogeneous reactions included in the CMAQ model and their uptake coefficients.

No.	Heterogeneous reactions	Uptake coefficient (γ) or reaction rate (k)	References
Original CMAQ			
OR1	$N_2O_5(g) + H_2O(cd) + \varphi^a Cl^-(cd) \rightarrow$ $\varphi^a(HNO_3(g) + ClNO_2(g)) + 2(1-\varphi^a)HNO_3(g)$	$\gamma_{N_2O_5} = 3.2\times10^{-8}k'\left(1-\frac{1}{\left(\frac{0.06[H_2O(l)]}{[NO_3^-]}\right)+1+\left(\frac{29[Cl^-]}{[NO_3^-]}\right)}\right)$ [b] $k' = 1.15\times10^6 - 1.15\times10^6 e^{[-0.13\times[H_2O(l)]]}$ [b]	Bertram and Thornton (2009)
OR2	$NO_2(g) \rightarrow 0.5HONO(g) + 0.5HNO_3(g)$	$k_{NO_2} = 5\times10^{-5}\times(S/V)$ S/V = surface to volume ratio	Kurtenbach et al. (2001)
OR3	$NO_3(g) \rightarrow HNO_3(g)$	1.0×10^{-4}	Mao et al. (2013)
Newly updated CMAQ			
NR1	$N_2O_5(g) + H_2O(cd) + \varphi^a Cl^-(cd) \rightarrow$ $\varphi^a(HNO_3(g) + ClNO_2(g)) + 2(1-\varphi^a)HNO_3(g)$	$\gamma_{N_2O_5} = 3.2\times10^{-8}k\left(1-\frac{1}{\left(\frac{0.06[H_2O(l)]}{[NO_3^-]}\right)+1+\left(\frac{29[Cl^-]}{[NO_3^-]}\right)}\right)$ [b] $k = 1.15\times10^6 - 1.15\times10^6 e^{[-0.13\times[H_2O(l)]]}$ [b]	Bertram and Thornton (2009)
NR2	$NO_2(g) \rightarrow 0.5HONO(g) + 0.5HNO_3(g)$	$k_{NO_2} = 5\times10^{-5}\times f_{RH}\times(S/V)$ $f_{RH} = \begin{cases} RH/50 & (RH<50) \\ RH/10-4 & (50\le RH<80) \\ 4 & (RH\ge80) \end{cases}$ $k_{NO_2} = 1\times10^{-3}\times\frac{Light\ intensity}{400}\times(S/V)$ RH = relative humidity S/V = surface to volume ratio	Fu et al. (2019)
NR3	$NO_3(g) \rightarrow HNO_3(g)$	1.0×10^{-3}	Jacob (2000)
NR4	$HO_2(g) \rightarrow 0.5H_2O_2(g)$	2.0×10^{-1}	Jacob (2000)
NR5	$OH(g) \rightarrow$ Products	1.0×10^{-1}	DeMore et al. (1997)
NR6	$O_3(g) \rightarrow$ Products	1.0×10^{-5}	Bauer et al. (2004)
NR7	$H_2O_2(g) \rightarrow$ Products	2.0×10^{-3}	de Reus et al. (2005)

[a] The yield of $ClNO_2$.

[b] $[H_2O(I)]$, $[NO_3^-]$, $[Cl^-]$ are the concentrations of particle liquid water, particulate nitrate, and particulate chloride, respectively.

Table S3. Set-up of sensitivity experiments for investigating the effects of changes in meteorological conditions and anthropogenic emissions on ozone variations.

Experiment	Description
M13E13	Modeling the summer of 2013 with MEIC 2013 anthropogenic emission
M14E14	Modeling the summer of 2014 with MEIC 2014 anthropogenic emission
M15E15	Modeling the summer of 2015 with MEIC 2015 anthropogenic emission
M16E16	Modeling the summer of 2016 with MEIC 2016 anthropogenic emission
M17E17	Modeling the summer of 2017 with MEIC 2017 anthropogenic emission
M14E13_BC13	Modeling the summer of 2014 with MEIC 2013 anthropogenic emission and 2013 chemical boundary condition from MOZART
M15E13_BC13	Modeling the summer of 2015 with MEIC 2013 anthropogenic emission and 2013 chemical boundary condition from MOZART
M16E13_BC13	Modeling the summer of 2016 with MEIC 2013 anthropogenic emission and 2013 chemical boundary condition from MOZART
M17E13_BC13	Modeling the summer of 2017 with MEIC 2013 anthropogenic emission and 2013 chemical boundary condition from MOZART
M13E14	Modeling the summer of 2013 with MEIC 2014 anthropogenic emission
M13E15	Modeling the summer of 2013 with MEIC 2015 anthropogenic emission
M13E16	Modeling the summer of 2013 with MEIC 2016 anthropogenic emission
M13E17	Modeling the summer of 2013 with MEIC 2017 anthropogenic emission

Table S4. Set-up of sensitivity experiments for investigating the impact of changes in biogenic emissions on ozone variations.

Experiment	Description
M13E13	Modeling the summer of 2013 with MEIC 2013 anthropogenic emission
M13E13_BIO14	M13E13 but with 2014 biogenic emission
M13E13_BIO15	M13E13 but with 2015 biogenic emission
M13E13_BIO16	M13E13 but with 2016 biogenic emission
M13E13_BIO17	M13E13 but with 2017 biogenic emission

Table S5. Set-up of sensitivity experiments for investigating the impact of changes of temperature, specific humidity, wind field, planetary boundary layer height, cloud, and precipitation on ozone variations.

Experiment	Description
M13E13	Modeling the summer of 2013 with MEIC 2013 anthropogenic emission
M13E13_TEMP17	M13E13 but with 2017 temperature
M13E13_SPHU17	M13E13 but with 2017 specific humidity
M13E13_WIND17	M13E13 but with 2017 wind field
M13E13_PBLH17	M13E13 but with 2017 planetary boundary layer height
M13E13_CLDF17	M13E13 but with 2017 cloud
M13E13_PREC17	M13E13 but with 2017 precipitation

Table S6. Set-up of sensitivity experiments for investigating the impact of changes in long-range transport on ozone variations.

Experiment	Description
M13E13	Modeling the summer of 2013 with MEIC 2013 anthropogenic emission
M13E13_BC14	M13E13 but with 2014 chemical boundary condition
M13E13_BC15	M13E13 but with 2015 chemical boundary condition
M13E13_BC16	M13E13 but with 2016 chemical boundary condition
M13E13_BC17	M13E13 but with 2017 chemical boundary condition

References:

Bauer, S. E., Balkanski, Y., Schulz, M., Hauglustaine, D. A., and Dentener, F.: Global modeling of heterogeneous chemistry on mineral aerosol surfaces: Influence on tropospheric ozone chemistry and comparison to observations, J Geophys Res-Atmos, 109, Artn D02304

10.1029/2003jd003868, 2004.

Bertram, T. H., and Thornton, J. A.: Toward a general parameterization of N2O5 reactivity on aqueous particles: the competing effects of particle liquid water, nitrate and chloride, Atmos Chem Phys, 9, 8351-8363, 2009.

de Reus, M., Fischer, H., Sander, R., Gros, V., Kormann, R., Salisbury, G., Van Dingenen, R., Williams, J., Zöllner, M., and Lelieveld, J.: Observations and model calculations of trace gas scavenging in a dense Saharan dust plume during MINATROC, Atmos. Chem. Phys., 5, 1787-1803, 10.5194/acp-5-1787-2005, 2005.

DeMore, W. B., Sander, S. P., Golden, D. M., Hampson, R. F., Kurylo, M. J., Howard, C. J., Ravishankara, A. R., Kolb, C. E., and Molina, M. J.: Chemical kinetics and photochemical data for use in stratospheric modeling, National Aeronautics and Space Administration and Jet Propulsion Laboratory, California Institute of Technology, California, 1997.

Fu, X., Wang, T., Zhang, L., Li, Q., Wang, Z., Xia, M., Yun, H., Wang, W., Yu, C., Yue, D., Zhou, Y., Zheng, J., and Han, R.: The significant contribution of HONO to secondary pollutants during a severe winter pollution event in southern China, Atmos. Chem. Phys., 19, 1-14, 10.5194/acp-19-1-2019, 2019.

He, J., Gong, S., Yu, Y., Yu, L., Wu, L., Mao, H., Song, C., Zhao, S., Liu, H., Li, X., and Li, R.: Air pollution characteristics and their relation to meteorological conditions during 2014–2015 in major Chinese cities, Environ. Pollut., 223, 484-496, https://doi.org/10.1016/j.envpol.2017.01.050, 2017.

Jacob, D. J.: Heterogeneous chemistry and tropospheric ozone, Atmos. Environ., 34, 2131-2159, 2000.

Kurtenbach, R., Becker, K. H., Gomes, J. A. G., Kleffmann, J., Lorzer, J. C., Spittler, M., Wiesen, P., Ackermann, R., Geyer, A., and Platt, U.: Investigations of emissions and heterogeneous formation of HONO in a road traffic tunnel, Atmos. Environ., 35, 3385-3394, 10.1016/s1352-2310(01)00138-8, 2001.

Mao, J. Q., Paulot, F., Jacob, D. J., Cohen, R. C., Crounse, J. D., Wennberg, P. O., Keller, C. A., Hudman, R. C., Barkley, M. P., and Horowitz, L. W.: Ozone and organic nitrates over the eastern United States: Sensitivity to isoprene chemistry, J Geophys Res-Atmos, 118, 11256-11268, 2013.

Tu, J., Xia, Z. G., Wang, H. S., and Li, W. Q.: Temporal variations in surface ozone and its precursors and meteorological effects at an urban site in China, Atmos Res, 85, 310-337, 10.1016/j.atmosres.2007.02.003, 2007.